

Velocity fields below the magnetic canopy of solar flux tubes: evidence for high-speed downflows?

C. Briand^{1,2} and S.K. Solanki³

¹ Instituto de Astrofísica de Canarias, E-38200 La Laguna, Tenerife, Spain

² THEMIS, I.A.C., E-38200 La Laguna, Tenerife, Spain

³ Institut für Astronomie, ETH-Zentrum, CH-8092 Zürich, Switzerland

Received 5 August 1997 / Accepted 28 October 1997

Abstract. It is well-established that velocities in the immediate surroundings of solar magnetic elements produce an asymmetry in the Stokes V profiles emerging from the magnetic feature. Conversely, the observed Stokes V asymmetry can be used to infer the velocity field. Taking as constraints the area asymmetries of the Stokes V profiles of two lines of neutral magnesium ($\lambda 457\text{nm}$ and $\lambda 517\text{nm}$) observed near the center of the solar disk, the (vertical) component of the velocity field below the magnetic canopy of flux tubes is investigated. We find that the strong Mg I b_2 line at 517nm qualitatively extends the diagnostic capabilities of Stokes V asymmetry, mainly due to the fact that it is sensitive to velocities over a large range of heights and hence also at relatively large distances from the flux tube axis. In order to retrieve the observed area asymmetry of both lines, up- as well as downflows have to be introduced in the models. If the temperature differences between the two flows are neglected then a downflow of $1.5 - 2\text{km s}^{-1}$ close to the edge of the flux tube and an almost equally strong upflow at greater distances (corresponding to the central part of a granule) reproduces the observed area asymmetries. If we take into account that the temperature in the downflow is lower than in the upflow, we can only reproduce the observations if the downflow is fast ($\geq 5\text{ km s}^{-1}$) and concentrated into narrow lanes.

Key words: Sun: faculae, plages – Sun: magnetic fields

1. Introduction

Asymmetries between the blue and red areas and amplitudes of Stokes V profiles (the Stokes parameter which describes the net circular polarization of light) are well known features. They may be parameterized by an area asymmetry δA between the blue (b) and red (r) lobes of Stokes V ($\delta A = \frac{A_b - A_r}{A_b + A_r}$) and a corresponding amplitude asymmetry δa ($\delta a = \frac{a_b - a_r}{a_b + a_r}$).

Send offprint requests to: C. Briand

Observations of plages and network at Sun center in general reveal $\delta A \geq 0$ and $\delta a \geq 0$ (Solanki & Stenflo 1984, 1985; Martínez Pillet et al. 1997). At the same time the zero-crossing wavelength of Stokes V is found to be shifted by less than 250 m s^{-1} (Stenflo et al. 1984; Stenflo & Harvey 1985; Solanki 1986; Martínez Pillet et al. 1997). Van Ballegooijen (1985) first suggested that a velocity field *outside* the magnetic flux tube can lead to area asymmetries of Stokes V without shifting the zero-crossing wavelength. Grossmann-Doerth et al. (1988, 1989) provided an analytical proof of van Ballegooijen's suggestion and they, together with Solanki (1989), showed that this mechanism produces asymmetry values of the correct magnitude. The idea may be summarized as follows: flux tubes expand with height forming what we shall call a magnetic canopy, i.e. field overlying a field-free atmosphere. Consider now a vertical ray passing through the canopy, the presence of a velocity field in the non-magnetic atmosphere below the canopy implies a shift of the line absorption profile before the radiation penetrates the flux tube. Together with the saturation of the line, this leads to a different absorption in the red and blue wings in the higher, magnetic layers of the atmosphere and thus an asymmetry in the Stokes V profile. For line that are not strongly Zeeman split, the crucial parameter determining the magnitude of the asymmetry is the ratio between the shift of the absorption profile due to the external velocity and the line width. Even a small amplitude flow can give rise to a high asymmetry if the line is narrow.

A downflow in the immediate surroundings of flux tube is expected due to the location of flux tubes in intergranular lanes, i.e. regions of converging and descending flow (e.g. Title et al. 1987) and to the inflow of radiation into the flux tube, which itself drives a downflow in the surroundings (Deinzer et al. 1984).

Relatively few quantitative studies of the production of Stokes V asymmetry have been carried out (e.g. Solanki 1989; Bünte et al. 1993; Sánchez Almeida et al. 1988, 1996; Bellot Rubio et al. 1997). In this paper we investigate how the Stokes V profiles of two lines of neutral magnesium ($\lambda 457\text{nm}$ and $\lambda 517\text{nm}$) can constrain the flow field in the non-magnetic re-

gion surrounding the flux tubes. Of particular interest is the Mg I b_2 line at 517nm, since it is considerably stronger than any other line whose asymmetry has previously been calculated. As we shall demonstrate it significantly extends the diagnostic potential of the Stokes V asymmetry. Information on the granular flow surrounding the flux tubes is obtained on the basis of these calculations and observed values of δA . These are the first NLTE calculations that attempt to reproduce observed Stokes V asymmetry. The large computational effort inherently required by NLTE calculations is mainly responsible for the relative simplicity of the model we consider.

The paper is structured as follows: Sect. 2 describes the numerical procedure to compute the Stokes parameters of the two Mg I lines in NLTE. In Sect. 3 we investigate the consequences of the presence of up- and downflows outside the flux tubes on the area asymmetries of the two lines. In Sect. 4 we study the implications of different temperatures in the up- and downflows on the Stokes V asymmetries, while the last section is dedicated to a discussion of these results and to possible improvements.

2. Observational data and numerical procedure

2.1. Observational data

The computed profiles are compared with Stokes I and V observations performed in the enhanced network with the Fourier Transform Spectrometer (FTS) (Stenflo et al. 1984). The spatial resolution of those observations is moderate ($10''$) and the integration time large. On the other hand, the spectral resolution is high (360000), the noise level is low ($1-2 \times 10^{-4} I_c$, where I_c is the continuum intensity) and the two spectral lines were observed strictly simultaneously.

The observed area asymmetry of the two lines is not trivial to determine. The wavelength range over which the V profiles are integrated must be fixed with great care in order to avoid the contribution of neighbouring and even blending lines, as in the case of Mg I b_2 . This is important because the derived properties of the atmosphere outside the flux tubes are strongly dependent on these values. The area asymmetry of the $\lambda 457\text{nm}$ Stokes V profile has been computed over $\pm 0.028\text{nm}$ from the line center (the constraint coming from the presence of another line near the red wing); that of the $\lambda 517\text{nm}$ Stokes V profile has been determined over $\pm 0.072\text{nm}$ (the constraint coming here from a blend in the blue wing). Since we estimate that over 99% of the area of the $|V|$ profile of $\lambda 457\text{nm}$ and over 95% of $\lambda 517\text{nm}$ lie within these limits we feel reasonably confident about the derived asymmetries. We obtain the following observed relative area asymmetry values: 0.108 ± 0.005 for the $\lambda 457\text{nm}$ line and 0.016 ± 0.006 for the $\lambda 517\text{nm}$ line.

2.2. Model and numerical procedure

We adopt a 2-component model composed of a magnetic flux tube embedded in a non-magnetic medium. The flux tube is in pressure equilibrium with its surroundings (the so-called thin-tube approximation; Parker 1974; Defouw 1976; Roberts & Webb 1978) and both are in hydrostatic equilibrium.

Due to the decreasing gas pressure the flux tube expands with height until it merges with a neighboring flux tube. In our model the merging height is determined primarily by the magnetic filling factor (i.e. the fraction of the solar surface covered by field at the level $z = 0$, i.e. $\tau_{500} = 1$ in the non-magnetic atmosphere), secondly by the thermal structure of the flux tube relative to its surroundings and finally by the field strength (cf. Solanki & Steiner 1990).

The numerical procedure adopted for the radiative transfer is the same as in Briand & Solanki (1995, hereafter Paper I). A cylindrical geometry is assumed. The atmosphere is cut by multiple rays (parallel to the axis of the flux tube) along which the non-LTE radiative transfer equation is solved to obtain the source functions and opacities as a function of height (assuming the field-free approximation, e.g. Rees 1969). These computations have been performed with a revised version of the code MULTI (Scharmer & Carlsson 1985; Carlsson 1986; Uitenbroek 1989). The ionisation equilibrium of hydrogen has not been recomputed for each ray, which means that the electron density in the flux tube is slightly different from its true value. We checked, however, that a decrease of the electron density by 20% in all layers of the atmosphere does not change the Stokes I profiles by more than 8%. Moreover, since the lower and middle photospheric layers of each atmosphere are well-described by LTE, the error in the electron density is considerably smaller than the tested 20%.

Then, using the output of MULTI, the Stokes parameters are computed with the code SPSR developed by Rees et al. (1989). The two Mg I lines are formed sufficiently deep to allow us to neglect radiative transfer perpendicular to the rays. Finally, profiles formed along individual rays are added together in order to simulate observations that do not resolve the flux tubes. All thermodynamical parameters (temperature, pressure, density, microturbulent velocity) are initially horizontally homogeneous in the flux tube and in the non-magnetic component of the atmosphere (Sect. 3). Two different flow velocities below the magnetic canopy, however are allowed. They are located at different distances from the flux tube axis, as will be described later. In Sect. 4 each flow component is associated with a different thermal structure.

A magnetic field strength of 1500 G at $\tau_{500}(\text{quiet Sun}) = 1$ is chosen, as suggested by spectral lines of iron at $\lambda 525.0\text{nm}$ and $\lambda 524.7\text{nm}$ present in the same FTS spectra as the Mg I lines. The filling factor α at $\tau_{500}(\text{quiet Sun}) = 1$ has also been deduced from iron-line observations. Its value has been fixed to 0.05.

2.2.1. Atmospheric models

The non-magnetic component of the atmosphere is described, at least initially, by the HSRA model (Gingerich et al. 1971), extended downwards. A height-independent microturbulence of 1 km s^{-1} is adopted.

The flux tube atmosphere is described by the network model NCHROM7 which was constructed in Paper I. Also following Paper I, the microturbulence velocity is fixed at 1.6 km s^{-1} . Macro-turbulent velocity has not been included. No flows are

considered inside the flux tube throughout this work. Consequently, all the calculated Stokes V profiles possess an unshifted zero-crossing wavelength. For our choice of filling factor and atmospheric models we find that the flux tubes merge at a height of 620 km.

In the present paper we describe the influence of two velocity components below the canopy on the Stokes V parameters of the two magnesium lines. We consider only vertical flows, a downflow and an upflow. Each velocity component occupies a ring surrounding the flux tube, with the downflow always being in the inner ring. Initially all considered velocities are height-independent and the temperature in both velocity components is exactly the same. We have also investigated the effect of 3 components of the external atmosphere (it includes an additional component between up- and downflow, which is at rest), but do not describe the results further, since they lead to no new insight.

2.2.2. Atomic model

The employed atomic model of neutral magnesium is the same as in Paper I. It is composed of 11 levels plus a continuum. A total of 15 transitions are included, all treated in complete frequency redistribution. All atomic parameters are equal to those used in Paper I. Stokes profiles are calculated for two spectral lines only, namely $\lambda 457\text{nm}$ and $\lambda 517\text{nm } b_2$. We list a few of their atomic parameters in Table 1. The first column indicates the wavelength in nanometers. The second column lists the transition, the third column the oscillator strength, the fourth column g_{eff} , the effective Landé factor, and the last column the type of the dipole transition. More details are to be found in Paper I.

Before proceeding, it is necessary to indicate at what height these lines are formed. As we shall see, most of the advantage of considering the two lines simultaneously stems from the fact that they are formed over very different height ranges. The $\lambda 457\text{nm}$ line is photospheric, with a source function in Local Thermodynamical Equilibrium (LTE), while the core of the $\lambda 517\text{nm}$ line is formed above the temperature minimum height in non-LTE (see Fig. 5 of Paper I). Thus, the $\lambda 457\text{nm}$ line is sensitive to the structure of the lower half of the photosphere only, while the latter is sensitive to the physical conditions at and below the merging height of the flux tubes.

Of course velocity response functions for the two lines would be more accurate indicators than the heights at which $\tau = 1$ is reached at different wavelengths in the line, but for the purposes of this paper it is sufficient to know the approximate height range of formation.

3. Results from an unperturbed thermal stratification

3.1. Tests calculations

We first present some simple test calculations which inspired us to develop an approximate analytical description of the influence of the flows on the two lines. These analytical solutions were needed in order to reduce the parameter space in which we need to search for a numerical solution that satisfies the observations.

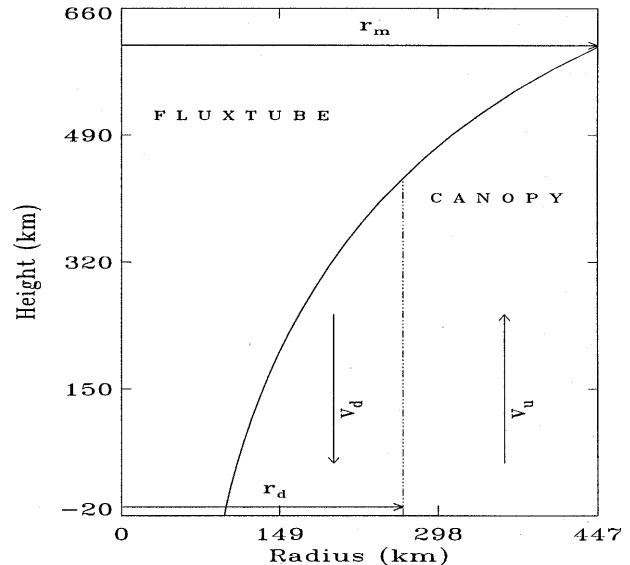


Fig. 1. Schematic plot of the geometry of the model. Plotted is a cut through the axially symmetric model. r_m indicates the maximum radius reached by the flux tube (which also corresponds to the outer radius of the upflow), r_d the outer radius of the downflow. The boundary between the downflowing (v_d) and upflowing (v_u) gas is marked by the dot-dashed line

We calculate line profiles for downflow-rings of varying width while keeping the remaining part of the non-magnetic region at rest. Such a set of calculations was carried out for velocities ranging from -1.0 up to -6.0 km s^{-1} (negative velocities correspond to downflows)¹.

Let us call r_d the radial coordinate of the outer boundary of the downflow region normalized to the radius of the flux tube at $z = 0$ (cf. Fig. 1). In Fig. 2 we plot the relative area asymmetry, δA , resulting from these calculations as a function of r_d . The two lines experience the velocity field very differently: the area asymmetry of the $\lambda 457\text{nm}$ line is mainly influenced by the velocity field close to the flux tube boundary, say for $r_d \leq 2$. Even strong flows hardly influence the area asymmetry of this line if they are situated far from the tube axis. The $\lambda 517\text{nm}$ line, on the other hand, is sensitive to the velocity field at all radii. The difference in the height of formation of the two lines underlies the difference of their behavior. Only the non-magnetic atmosphere located at or below the height range of formation of the Stokes V profile has any influence on it. Since the $\lambda 457\text{nm}$ line is formed in the lower half of the photosphere, which is typical for lines of its strength, only the flows close to the flux tube play a significant rôle. On the other hand, the Stokes V profile of the $\lambda 517\text{nm}$ line is formed over a wide range of heights reaching up to the merging height of the flux tube and thus is sensitive to the influence of any velocity fields present in the non-magnetic

¹ This choice of flow direction is not critical for these test calculations: the area asymmetries obtained with upflows have just the opposite sign, but the same magnitude

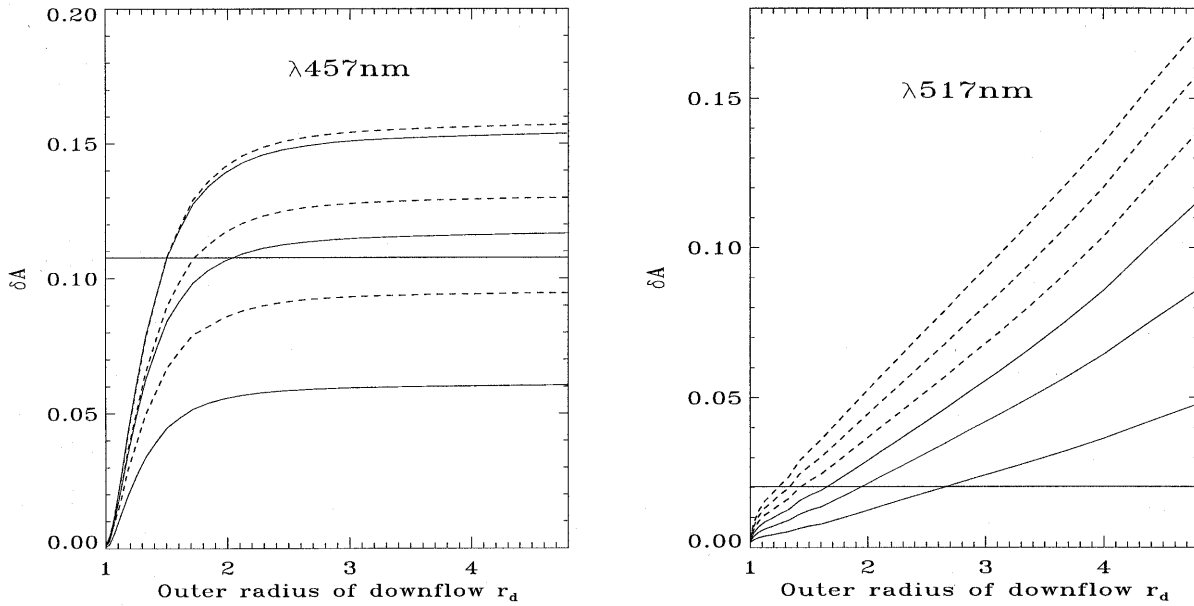


Fig. 2. Relative area asymmetry vs. r_d (cf. text). Each curve represents the results for a given downflow velocity. Solid curves: $-1, -2, -3 \text{ km s}^{-1}$ (from bottom to top); Dashed curves: $-4, -5, -6 \text{ km s}^{-1}$ (from top to bottom for $\lambda 457 \text{ nm}$ and bottom to top for $\lambda 517 \text{ nm}$). In each case, the horizontal solid line represents the observed area asymmetry

Table 1. Atomic parameters adopted for the computation of the two Mg I lines

Wavelength (nm)	Label	f	g_{eff}	Dipole transition
457.11	$3s3p \ ^3P_0$ to $3s^2 \ ^1S_0$	3.55×10^{-6}	1.50	Magnetic
517.27	$3s4s \ ^3S_1$ to $3s3p \ ^3P_1$	1.37×10^{-1}	1.75	Electric

component. In particular, its δA depends almost linearly on the radius of the downflow ring.

Another important property is visible in Fig. 2: up to a downflow velocity of -4 km s^{-1} the area asymmetry of the $\lambda 457 \text{ nm}$ line increases as the velocity modulus increases, while for higher values it decreases. Since the $\lambda 457 \text{ nm}$ line is weak and hence relatively narrow, the Doppler shift due to the downflow falls outside the unshifted line already for relatively low velocities (i.e. $\geq 4 \text{ km s}^{-1}$), thus reducing the area asymmetry (cf. Grossmann-Doerth 1989). The same also happens for $\lambda 517 \text{ nm}$, but at a much higher (absolute) velocity since the line is broad. For absolute velocities less than 6 km s^{-1} this line shows no reduction in asymmetry with increasing velocity, although there are signs of a saturation. In the following, we call the domain of velocities for which the area asymmetry of the $\lambda 457 \text{ nm}$ line increases with the absolute value of the downflow the “low velocity regime” (i.e. $|\text{velocity}| \leq 4 \text{ km s}^{-1}$), while larger velocities are counted to the “high velocity regime”.

3.2. Analytical solutions

We took advantage of the properties of the test calculations to derive empirical equations which describe the dependence of the area asymmetry of each line on the velocities and areas covered by up- and downflows. Let us r_m the outer radius of the computational domain (i.e. the radius of the flux tube above

the merging height; $r_m^2 = \frac{1}{\alpha}$) normalized to the radius of the flux tube at $z = 0$ (cf. Fig. 1), δA_{457} and δA_{b_2} the *observed* area asymmetry of the Stokes V profiles of the two lines, δA_{457}^c and $\delta A_{b_2}^c$ the respective *computed* area asymmetries, and v_d and v_u the down- and upflow velocities, respectively. r_d and r_m are independent of height. The inner boundary of the downflow is given by the boundary of the flux tube (which does depend on height). In the “low velocity regime” it is straightforward to write empirical relations between δA of the two lines and the flow parameters.

Fig. 2 suggests the following simple and approximate equation for the $\lambda 517 \text{ nm}$ line:

$$-\delta A_{b_2}^c = g v_d (r_d - 1) + g v_u (r_m - r_d). \quad (1)$$

where g is a constant of proportionality.

The equation for the other line is more complex. Indeed, two regimes have to be considered: if $r_d < 1.5$, then the area asymmetry increases almost linearly with r_d , whereas for $r_d > 2$ the area asymmetry is almost independent of r_d . For intermediate values the dependence on r_d is non-linear. For simplicity we count this r_d range to the first regime. Then we obtain approximately:

$$-\delta A_{457}^c = h v_d (r_d - 1) + h v_u (2 - r_d) \quad \text{if } r_d < 2, \quad (2)$$

$$-\delta A_{457}^c = h v_d \quad \text{if } r_d > 2. \quad (3)$$

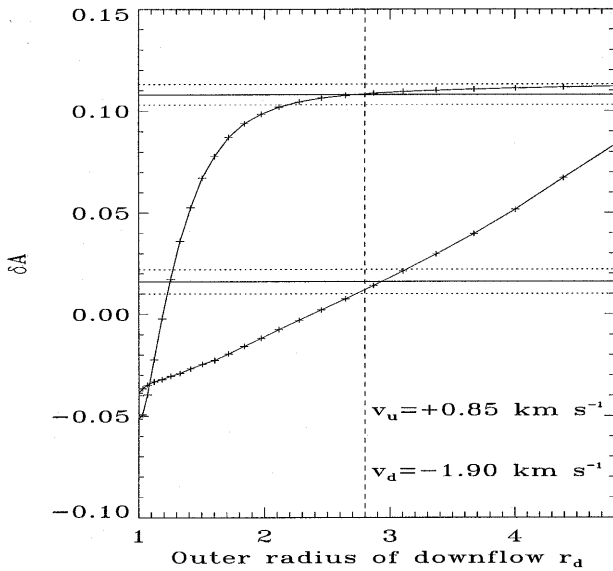


Fig. 3. Area asymmetry δA of the $\lambda 457\text{nm}$ line (upper curve) and $\lambda 517\text{nm}$ line (lower curve) vs. r_d . The horizontal solid lines represent the observed values of the area asymmetry while the dotted lines indicate their $\pm 1\sigma$ uncertainty. The vertical line shows the r_d location where the mass conservation is satisfied ($r_d = 2.80$)

The coefficients g and h are deduced empirically from Fig. 2 (for which $v_u = 0$), i.e.

$$g = \frac{-\delta A_{b_2}^c}{v_d (r_d - 1)}, \quad (4)$$

and

$$h = \frac{-\delta A_{457}^c}{v_d (r_d - 1)} \quad \text{if } r_d < 2, \quad (5)$$

$$h = \frac{-\delta A_{457}^c}{v_d} \quad \text{if } r_d > 2. \quad (6)$$

By averaging the results obtained from different velocities and radii we get $g = 0.011 \pm 0.002$, $h = 0.070 \pm 0.003$ for $r_d \leq 2$ and 0.057 ± 0.003 for $r_d \geq 2$.

The v_u , v_d and r_d constitute the three unknowns of the set of equations. To close the system we impose mass conservation. Indeed, Hasan & Schüssler (1985) provide a theoretical estimate of the order of magnitude of the inflow into the flux tube from the non-magnetic region: 10 cm s^{-1} . Compared to other velocities involved in these calculations, this inflow can be neglected. In principle we should impose mass conservation at each height of the atmosphere. However, since the velocities as well as the radii r_d and r_m are considered height independent throughout this work, it has rather been imposed at a representative height. The corresponding flux tube radius relative to its radius at $z = 0$ is called X :

$$\rho_d v_d (r_d^2 - X^2) = -\rho_u v_u (r_m^2 - r_d^2). \quad (7)$$

The relative radius X has been fixed to 1.5 which represents a height of 170 km in the non-magnetic atmosphere, roughly

in the middle of the formation heights of the maxima of the V profiles of the two lines. This parameter is not very critical, as long as we remain around the middle of the region of formation of the $\lambda 457\text{nm}$ line. Note that as long as the external atmosphere is horizontally isothermal, the densities ρ_u and ρ_d are equal, so that they need not be explicitly known to satisfy Eq.(7). Finally, we also make use of the relationship $r_m = \frac{1}{\sqrt{\alpha}}$, whereby α is known from the observations.

The solution in the case $r_d > 2$ is given by

$$r_d = \frac{-X^2 + \frac{1}{\sqrt{\alpha}} \left(1 + \frac{\delta A_{b_2}}{\delta A_{457}} \frac{h}{g}\right)}{-1 + \frac{1}{\sqrt{\alpha}} - \frac{\delta A_{b_2}}{\delta A_{457}} \frac{h}{g}}, \quad (8)$$

$$v_d = -\frac{\delta A_{457}}{h}, \quad (9)$$

$$v_u = \frac{\delta A_{457}}{h} \frac{r_d^2 - 1}{r_m^2 - r_d^2}. \quad (10)$$

The solution for that case is $r_d = 2.05 \pm 1.31$, $v_u = +0.32 \pm 0.66 \text{ km.s}^{-1}$ and $v_d = -1.90 \pm 0.19 \text{ km.s}^{-1}$. The uncertainties have been determined taking into account the errors on the parameters h and g and the observed area asymmetries.

Similar equations can be found for the case $r_d < 2$. However, the solution turns out to be unphysical, once the numerical values of the various known parameters are introduced, since the boundary between the two flows is located at the edge of the flux tube.

Finding analytical expression for the high velocity regime is more tricky because δA of $\lambda 457\text{nm}$ does not react linearly to v_d . For velocities close to -4 km s^{-1} we have decided not to include an equation describing the behavior of δA_{457} , so that we cannot determine a unique solution, but rather can only express the remaining parameters in term of the downflow velocity. The test calculations suggest that the parameter $g = 0.008$. For downflow values lying between -4.5 and -6.0 km s^{-1} we obtain negative values for v_u , which once again is unphysical. For higher downflow velocity, the above equations cannot be used anymore since the dependence of the area asymmetry of the $\lambda 517\text{nm}$ on velocity begins to change. No solution is found for $r_d > 2$ and large downflow velocities.

In summary, within the limitations of our analytical approximation, the observations allow only one scenario, namely almost equal v_u and v_d , each covering approximately the same surface area. Note that only by considering both a weak line like $\lambda 457\text{nm}$ and the strong Mg I b_2 line can one limit the choice to this possibility. The δA of only one of these lines on its own can be reproduced by an infinite number of velocity combinations.

3.3. Numerical solution

The analytical solution presented in Sect. 3.1 served as the starting point for numerical computations of the Stokes profiles. The aim of the present calculations is to test the diagnostic capabilities of δA of the Mg I lines, and in particular to test the analytical predictions made in Sect. 3.1. The geometry of the flows remains unchanged.

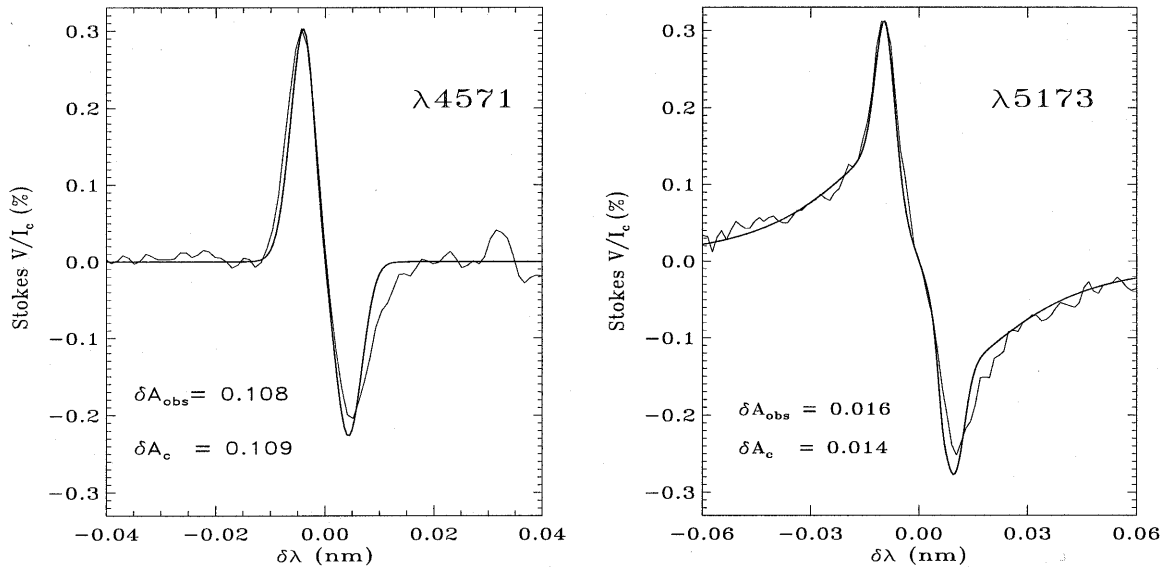


Fig. 4. Comparison between observed (thin) and computed (thick) V profiles. The parameters underlying the computations are $r_d = 2.95$, $v_u = +0.85 \text{ km s}^{-1}$ and $v_d = -1.90 \text{ km s}^{-1}$

3.3.1. Low velocity regime

We found no combination of flows in the low velocity regime with $r_d < 2$ which reproduced the observations and conserved mass, in agreement with the analytical prediction.

In the case $r_d > 2$ we again confirmed the analytical prediction. The observed δA values were reproduced within the limits of the observed accuracy by the combination $v_u = +0.9 \pm 0.5 \text{ km s}^{-1}$, $v_d = -1.9 \pm 0.1 \text{ km s}^{-1}$ and $r_d = 3.0 \pm 0.4$. The computations also confirmed the uncertainties in these parameters: the choice on v_d is very restricted, while a larger range of upflow values is available. Fig. 3 displays the variations of δA of both lines vs. r_d for the best combination of flows. Observed and computed Stokes V profiles are compared in Fig. 4. The remaining discrepancy (especially in the red wings of the profiles) once more confirms that a single set of flows outside the flux tubes alone cannot simultaneously reproduce area and amplitude asymmetries of V profiles. The additional amplitude asymmetry of observed profiles may be due to waves in the flux tubes (Grossmann-Doerth et al. 1991; Solanki & Roberts 1992), a combination of different downflows around many small magnetic features (Sánchez Almeida et al. 1996), or if we neglect mass conservation, to steady flows within the flux tube (Bellot Rubio et al. 1997).

3.3.2. High velocity regime

Yet again, the numerical solutions fully support the analytical predictions: we have not been able to find a combination of flow which satisfies at the same time the area asymmetry of both lines and the mass conservation law, although we considered a wide range of model parameters.

4. Results for different up- and downflow temperatures

The δA of temperature-sensitive lines (such as the Mg I lines we consider) depends significantly on the temperature in the non-magnetic surroundings. The downflows around the flux tubes are known to be cooler than upflows. This follows from observations (Title et al. 1987), simulations Steiner et al. (1996) and empirical modeling (Solanki 1989; Bünte et al. 1993). Thus we need to include different up- and downflow temperatures into our model. In this section we investigate their influence on the area asymmetries of the Stokes V profiles of the two Mg I lines.

4.1. Test calculations

We have tested the influence of downflow temperature on δA . In the low velocity regime the δA of both lines decreases as the temperature of the downflow is decreased. This can be understood by considering the results of Grossmann-Doerth et al. (1989) that δA is largest when the Doppler shift Δ_D induced by the velocity of the downflow is of the same magnitude as the larger of the two quantities: the half width of the line Δ_L and the Zeeman shift Δ_Z . In our case, the Δ_L of both lines is much larger than Δ_Z .

In the low velocity regime Δ_D is smaller than the half width. With decreasing temperature the width of both lines increases. Consequently, the difference between Δ_D and Δ_L increases with decreasing temperature, thus decreasing the δA of both lines.

In the high velocity regime the δA of the two lines exhibits opposite temperature dependences, as can be seen from Fig. 5. In this figure, all curves are due to the same velocity pair ($v_d = -5 \text{ km s}^{-1}$, $v_u = 0 \text{ km s}^{-1}$). They differ only in the temperature of the downflow. Whereas the area asymmetry of the $\lambda 457 \text{ nm}$ increases (becomes more positive) with decreasing

temperature, δA_{517} decreases. The Δ_D $\lambda 457\text{nm}$ is now much larger than its half width Δ_L (this is confirmed by Fig. 2). Decreasing the temperature increases Δ_L which gets closer to Δ_D . Thus δA_{457} increases with decreasing temperature. On the other hand, even in this high velocity regime, $\Delta_D < \Delta_L$ of $\lambda 517\text{nm}$. The situation for this line is thus qualitatively unchanged relative to the low velocity regime. Consequently, δA_{517} decreases as the temperature is lowered.

We consider downflows cooler than the quiet Sun by up to 300K. This range of values is suggested by the results of Solanki (1989) from fits to the observed δA of Fe I lines of different strength and temperature sensitivity. The temperature of the upflow is constrained by the continuum contrast between regions containing magnetic features and those without. We employ only the contrast averaged over the whole network element, i.e. over flux tubes and non-magnetic surrounding, as suggested by the spatial resolution of $10''$ of our data. Since there is no information on the continuum contrast in the present set of observations, we have extracted it from publications. The values derived from high spatial resolution vary by a large amount. Such observations give continuum contrasts lying between 0.98 and 1.8 (e.g., Muller & Keil 1983; del Toro Iniesta et al. 1990). Low spatial resolution observations give contrast values much closer to 1 (Foukal & Fowler 1984; Lawrence 1988; Topka et al. 1992). We therefore require that the spatially averaged continuum-intensity of the whole modelled region (including the contribution of the flux tube and the non-magnetic atmosphere below the canopy) is equal to the quiet Sun continuum intensity. Thus:

$$S_{ft} \cdot I_{ft}^c + S_d \cdot I_d^c + S_u \cdot I_u^c = S_{qs} \cdot I_{qs}^c, \quad (11)$$

with I_x^c the continuum intensity, where subscript $x = ft$ stands for flux tube, d for downflow, u for upflow and qs for quiet Sun. Similarly, S_x denotes the surface area covered by the different regions.

Since the temperature of the quiet Sun and of the flux tube, as well as the area covered by each flow are known quantities (or can be derived), by fixing the temperature of either the up- or the downflow (i.e. T_u or T_d) we can deduce the remaining temperature. The electron pressure is computed consistently for the perturbed atmospheric models assuming LTE using the code of Gustafsson (1973). The microturbulent velocity is kept unchanged. We prescribe T_d and assuming black-body radiation obtain for T_u :

$$T_u = \frac{\beta}{\ln \left(\frac{r_m^2 - r_d^2}{r_m^2 \exp(-\frac{\beta}{T_{qs}}) - \exp(-\frac{\beta}{T_{ft}}) - (r_d^2 - 1) \exp(-\frac{\beta}{T_d})} \right)}, \quad (12)$$

where

$$\beta = \frac{h c}{k \lambda}, \quad (13)$$

with h being Planck's constant, c the speed of light, k Boltzmann's constant and λ the wavelength.

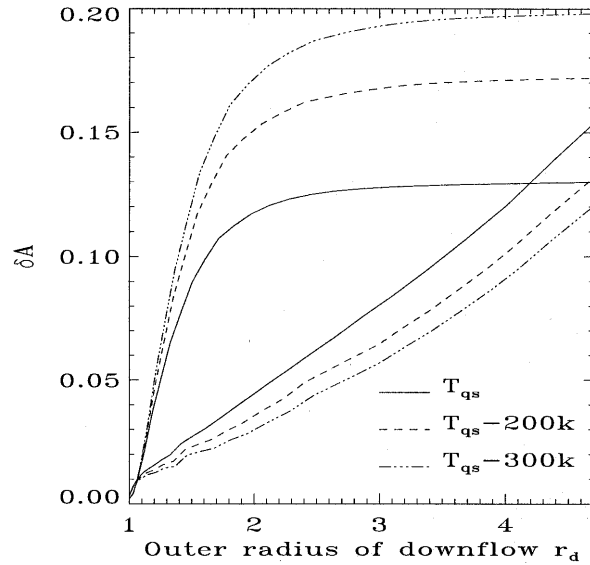


Fig. 5. Area asymmetry vs. r_d . $v_d = -5.0 \text{ km s}^{-1}$ while the remaining part of the non-magnetic atmosphere is at rest. Upper set of curves: 457nm line; lower curves: 517nm line

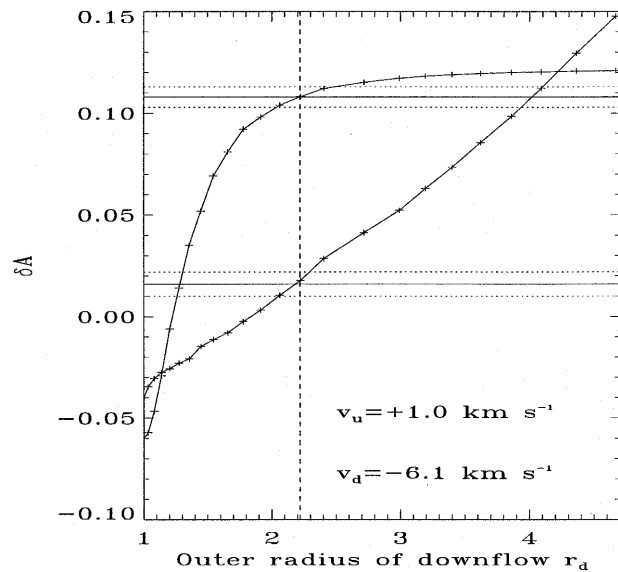


Fig. 6. Same as Fig. 3 when the temperature of the downflow is decreased by 200K relative to the quiet Sun. $r_d = 2.25$

Modifying the temperature of the non-magnetic atmosphere changes the shape of the flux tube boundary and hence also the merging height, since the scale height of the gas pressure scales with the temperature. We have taken these perturbations into account in our computation of the flux tube structure. However, in the range of temperatures we have used, the merging height turns out to vary by less than the vertical grid scale of the atmospheric models, probably because the more rapid expansion of the flux tube induced by the cool downflow is largely compensated by the slower expansion over the warm upflow.

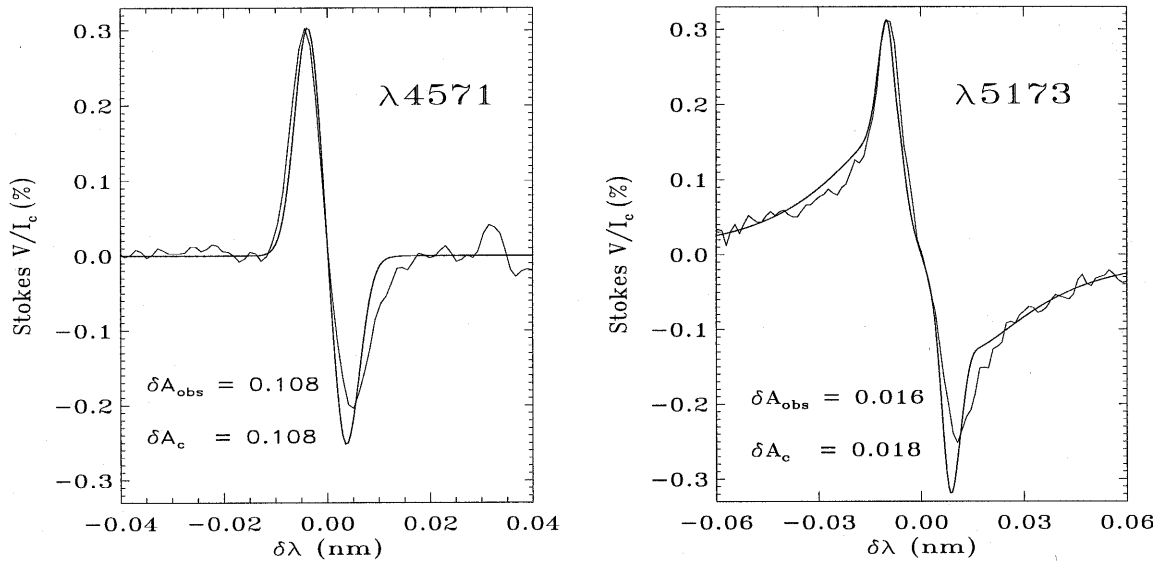


Fig. 7. Comparison of the observed and best fit computed Stokes V profiles for the case depicted in Fig. 6.

In the low velocity regime the parameter r_d is critical in fixing T_u with Eq.(12) because the area covered by each flow is of the same magnitude. Nevertheless, no low velocity model was found which reproduced the observations and conserved mass, even when the total continuum intensity was allowed to differ by a few percent from I_{qs}^c . In the high velocity regime, r_d has much less influence on the temperature structure. It was also possible to find a model reproducing the observations. We therefore restrict the rest of the discussion to this velocity regime.

We have searched and found numerical solutions for downflows that are up to 300K cooler than the quiet Sun. An example of a solution for a 200K cooler downflow is exhibited in Fig. 6. Plotted is the δA of both lines vs. r_d for the velocity pair $v_d = -6.1 \text{ km s}^{-1}$ and $v_u = 1.0 \text{ km s}^{-1}$. δA of both lines is reproduced for $r_d = 2.25$, which satisfies mass conservation. Eq. (12) gives an upflow temperature that is only a few degrees hotter than the temperature of the quiet Sun. Fig. 7 displays the Stokes V profiles of the two lines for this solution. Cooler downflows are possible, but the observations can then only be reproduced by even higher velocity values, lying closer to the sound speed, which would require us to abandon the assumption of hydrostatic equilibrium.

5. Conclusions

The consequences of the presence of flows in the field-free regions surrounding solar magnetic flux tubes have been qualitatively investigated by Grossman-Doerth (1988) and quantitatively with iron lines by Solanki (1989), Bünte et al. (1993) and Bellot Rubio et al. (1997). In this paper we show that the additional use of the Mg I b_2 line significantly extends the diagnostic capabilities of δA to constrain the atmosphere surrounding the magnetic elements. It constitutes also the first NLTE calculations that aim at quantitatively reproducing observed Stokes V asymmetries.

Solanki (1989) showed that by combining lines of different strength (all of which were considerably weaker than Mg I 517nm, however) and temperature sensitivity it was possible to deduce the temperature of the downflow lanes surrounding the flux tubes. Combining his results with our lines (and making use of spatially averaged continuum observations of plages) we show that almost unique values of the up- and downflows velocities (and the associated temperature structures) are obtained, within the limitations of our simple model. In particular, the observations suggest that the cool downflows bordering the flux tubes are concentrated into narrow lanes and have a high velocity of 5-7 km s^{-1} , while the upflows are warm, broad and comparatively gentle (1.5 km s^{-1}). This result agrees well with the simulations of Steiner et al. (1996).

It is likely that on the Sun the up- and downflow velocities in granules bordering flux tubes are not unique but vary radially and vertically (and probably also with time). The two velocities we find are therefore averaged in the sense that they produce a Doppler shift of the I profile formed under the canopy that is equivalent to the average Doppler shift produced by the distribution of up- and downflow velocities.

In a future step fits to the full Stokes I and V profile shapes should be attempted, including fits to the V amplitude asymmetry. Such fits have been made to other lines by Solanki (1989), Grossmann-Doerth et al. (1991), Sánchez Almeida et al. (1988) and Bellot Rubio et al. (1997). Stokes I profiles and in particular their bisectors should also be included in a future analysis. The I profiles are not particularly well reproduced by our current model (especially in the high velocity regime) not surprising in view of its simplicity. Introducing a height dependence of the velocity is the first step to improve the shape of the I profile. Such fits, particularly when constrained to satisfy mass and magnetic flux conservation, should allow the properties of the

non-magnetic surroundings of solar magnetic elements to be determined with greater accuracy and in finer detail.

References

- Bellot Rubio, L.R., Ruiz Cobo, B., Collados, M., 1997, *ApJ*, 478, L45
 Briand, C., Solanki, S.K., 1995, *A&A* 299, 596
 Bünte, M., Solanki, S. K., Steiner, O., 1993, *A&A*, 268, 736
 Carlsson, M., 1986, A Computer Program for Solving Multi-Level Non-LTE Radiative Transfer Problems in Moving or Static Atmospheres, Uppsala Astronomical Observatory Report 33
 Defouw, R.J., 1976, *ApJ.*, 209, 266
 Deinzer, W., Hensler, G., Schüssler, M., Weisshaar, E., 1984, *ApJ*, 139,435
 Foukal, P., Fowler, L., 1984, *ApJ*, 281, 442
 Gingerich, O., Noyes, R.W., Kalkofen, W., Cuny, Y., 1971, *Solar Phys.*, 18, 347
 Grossmann-Doerth, U., Schüssler, M., Solanki, S.K., 1988, *A&A*, 206, L37
 Grossmann-Doerth, U., Schüssler, M., Solanki, S.K., 1989, *A&A*, 221, 338
 Grossmann-Doerth, U., Schüssler, M., Solanki, S.K., 1991, *A&A*, 249, 239
 Hasan, S.S., Schüssler, M., 1985, *A&A*, 151, 69
 Lawrence, J.K., 1988, *Solar Phys.*, 116, 17
 Martínez Pillet, V, Lites, B.W., Skumanich, A., 1997, *ApJ*, 474, 810
 Müller, R., Keil, S.L., 1983, *Solar Phys.*, 87, 243
 Parker, E.N., 1974, *ApJ.*, 191, 245
 Rees, D.E., 1969, *Solar Phys.*, 10, 268
 Rees, D.E., Murphy, G.A., Durrant, C.J., 1989, *ApJ*, 339, 1093
 Roberts, B., Webb, A.R., 1978, *Solar Phys.*, 56, 5
 Sánchez Almeida, J., Collados, M., del Toro Iniesta, J.C., 1988, *A&A*, 201, L37
 Sánchez Almeida, J., Landi Degl'Innocenti, E., Martínez Pillet, V., Lites, B., 1996, *ApJ*, 466, 537
 Scharmer, G.B., Carlsson, M., 1985, *J. comput. Phys.*, 59, 66
 Solanki, S.K., 1986, *A&A*, 168, 311
 Solanki, S.K., 1989, *A&A*, 224, 225
 Solanki, S. K., Roberts, B., 1992, *M.N.R.A.S.*, 256, 13
 Solanki, S.K., Steiner, O., 1990, *A&A*, 243, 519
 Solanki, S.K., Stenflo, J.O., 1984, *A&A*, 140, 185
 Solanki, S.K., Stenflo, J.O., 1985, *A&A*, 148, 123
 Steiner, O., Grossmann-Doerth, U., Schüssler, M., Knölker, M., 1996, *Solar Phys.*, 164, 223
 Stenflo, J.O., Harvey, J.W., Brault, J.W., Solanki, S.K., 1984, *A&A*, 131, 333
 Stenflo, J.O., Harvey, J.W., 1985, *Solar Phys.* 95, 99
 Title, A.M., Tarbell, T.D., Topka, K.P., 1987, *ApJ*, 317, 892
 Topka, K.P., Tarbell, T.D., Title, A.M., 1992, *ApJ*, 296, 351
 del Toro Iniesta, Collados, M., Sánchez Almeida, J., Martínez Pillet, V, et al., 1990, *A&A*, 233, 570
 Uitenbroek, H., 1989, *A&A*, 216, 310
 van Ballegooijen, A.A., 1985, in *Theoretical Problems in High Resolution Solar Physics*, ed. H.U. Schmidt, Max-Planck-Inst. f. Astrophys., Munich, p. 177